OPEN
Toroidal vortices of light

Chenhao Wan [1,2], Qian Cao[1], Jian Chen[1], Andy Chong [3 ✉] and Qiwen Zhan [1 ✉]

Toroidal vortices, also known as vortex rings, are whirling, closed-loop disturbances that form a characteristic ring shape in liquids and gases and propagate in a direction that is perpendicular to the plane of the ring. They are well-studied structures and commonly found in various fluid and gas flow scenarios in nature, for example in the human heart, underwater air bubbles and volcanic eruptions[1-3]. Here we report the experimental observation of a photonic toroidal vortex as a new solution to Maxwell's equations, generated by the use of conformal mapping[4-7]. The resulting light field has a helical phase that twists around a closed loop, leading to an azimuthal local orbital angular momentum density. The preparation of such an intriguing state of light may offer insights for exploring the behaviour of toroidal vortices in other disciplines and find important applications in light–matter interactions, optical manipulation, photonic symmetry and topology, and quantum information[8-17].

Toroidal vortices, also known as vortex rings, are intriguing propagating ring-shaped structures with whirling disturbances rotating about the ring. Toroidal vortices are not uncommon in nature and science. Indeed, aquarium visitors are often amazed at how dolphins master creating and playing with bubble rings, which are air-filled vortex rings propagating in water. The scientific investigation of vortex rings dates back to 1867, when Lord Kelvin proposed the vortex atom model[18]. After one and a half centuries, vortex rings are still being actively investigated in a variety of disciplines. For example, in meteorology, vortex rings of wind, rain and hail are tightly related to the development of microbursts, which pose a great threat to aviation safety[19]. In cardiology, asymmetric redirection of blood flow through the heart resembles a toroidal vortex[1]. In magnetics, the experimental observation of vortex rings in a bulk magnet has only just been accomplished, opening up possibilities for studying complex three-dimensional (3D) solitons in bulk magnets[20]. In photonics and light science, there have been studies on toroidal dipole and multipole excitation in metamaterials[12-17]. However, the theory and experimental demonstrations of a propagating photonic toroidal vortex remain elusive. In this Article we fill this gap, based on conformal mapping. Conformal mapping is an angle-preserving transformation that has been utilized to bend optical rays with metamaterials in mapped directions to circumvent hidden objects so as to achieve optical cloaking[21,22]. Here we exploit conformal mapping to reshape a photonic vortex tube into a toroidal vortex. The photonic toroidal vortex is an approximate solution to Maxwell's equations and can propagate without distortion in a uniform medium with anomalous group velocity dispersion (GVD). The observation of a photonic toroidal vortex, like its counterparts in other disciplines, will open up a wealth of physical mechanisms to explore, such as toroidal electrodynamics, toroidal plasma physics, complex symmetry and topology for light confinement, sensing and manipulation, and interaction of light with metamaterials. The discovery of photonic toroidal vortices may also open up possibilities for the development of novel laser designs, as well as energy and information transfer methods.

The electric field of an optical wave packet is expressed as the product of the carrier at the central frequency and the envelope function. Under a scalar, paraxial and narrow bandwidth approximation, the envelope function that describes the dimensionless light field in a uniform medium with anomalous GVD is given by[23]

$$\frac{\partial^2 \Psi}{\partial x^2} + \frac{\partial^2 \Psi}{\partial y^2} + \frac{\partial^2 \Psi}{\partial \tau^2} + 2i\frac{\partial \Psi}{\partial z} = 0, \qquad (1)$$

where Ψ is the scalar wavefunction, x and y are the normalized transverse coordinates, τ is the normalized retarded time, and z is the propagation distance. The reason why the envelope function is expressed in a dimensionless way is to conveniently unify the spatial and temporal coordinates and derive a stable solution in the spatiotemporal domain. Anomalous GVD is chosen so as to obtain the same sign for the spatial and temporal second derivatives. As demonstrated by Supplementary equation (14), a spatiotemporal Laguerre–Gauss tube with the vortex line directed in the y direction is a solution to equation (1). The iso-intensity surface of a spatiotemporal Laguerre–Gauss tube is labelled at position 0 in Fig. 1. According to conformal mapping theory, the complex exponential function corresponds to a log-polar-to-Cartesian coordinate transformation. This conformal mapping transforms a line to a circle in two dimensions and performs a tube-to-toroidal mapping in 3D space. Here we adopt an afocal system that consists of two computer-generated phase masks to perform optical conformal mapping $(x, y) \mapsto (u, v)$, where (x, y) and (u, v) are the Cartesian coordinates in the planes at which the two phase elements are located. The log-polar-to-Cartesian coordinate transformation requires $u = b \exp\left(-\frac{x}{a}\right) \cos\left(\frac{y}{a}\right)$ and $v = b \exp\left(-\frac{x}{a}\right) \sin\left(\frac{y}{a}\right)$. The first phase mask performs the mapping from a tube to a toroid, and its phase profile can be derived through stationary phase approximation as[4,5]

$$\phi_1(x, y) = \frac{k}{d}\left[-ab \exp\left(-\frac{x}{a}\right) \cos\left(\frac{y}{a}\right) - \frac{x^2 + y^2}{2}\right], \qquad (2)$$

where k is the wave number, d is the distance between the two phase masks, and a and b are used to adjust the beam size and position in the (u, v) plane. The simulated evolution process for the mapping from a tube to a vortex ring in free-space propagation is labelled at positions from 1 to 5 in Fig. 1. The second phase mask recollimates the light. In the time-reversal direction, the second phase
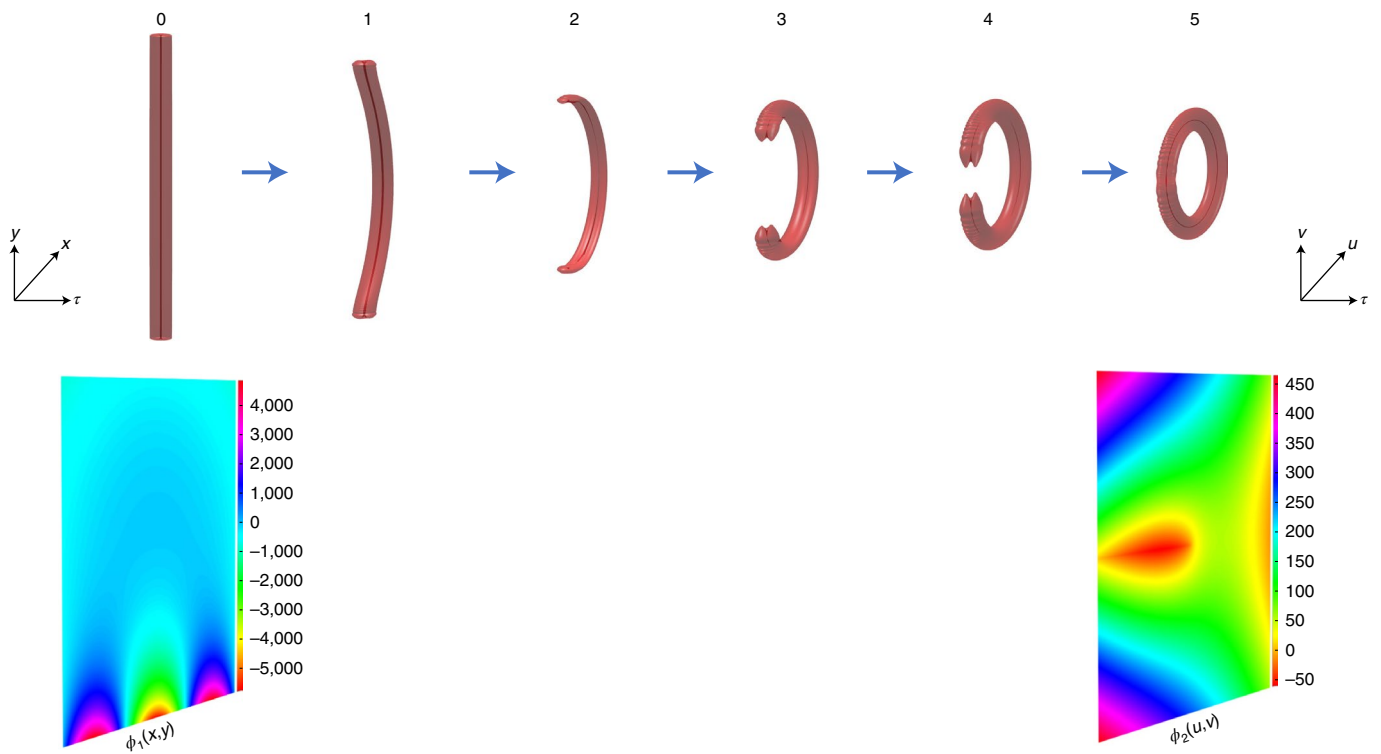
Fig. 1 | Simulation of the conformal mapping from a spatiotemporal vortex tube to a vortex ring. The spatiotemporal vortex tube acquires phase $\phi_1(x, y)$ and begins the transformation process in free-space repropagation. After completion of vortex ring formation, a second phase mask $\phi_2(u, v)$ is applied to collimate the light. The colour scale represents the value of the unwrapped phase.
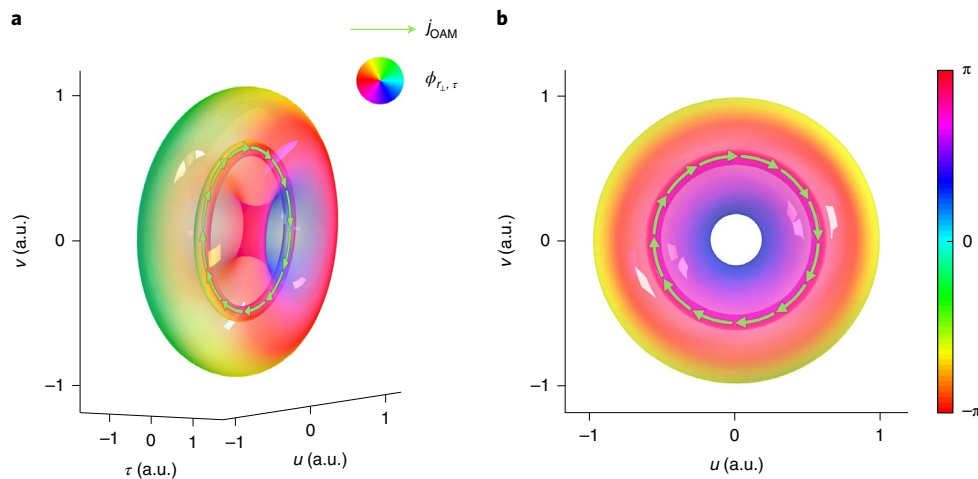

Fig. 2 | Intensity and phase information of a simulated photonic toroidal vortex. a, Side view of the 3D iso-intensity profile of a photonic toroidal vortex. The colours denote the rotating spatiotemporal spiral phase ($\Phi_{r_\perp, t}$). The topological charge of the spiral phase is 1. The direction of local OAM density (j_{OAM}) is marked with arrows. **b**, Front view of the iso-intensity profile of a photonic toroidal vortex.

mask performs a Cartesian-to-log-polar coordinate transformation. Similarly, its phase profile can be derived as

$$\phi_2(u, v) = \frac{k}{d}\left[-au\ln\frac{\sqrt{u^2+v^2}}{b} + av\arctan\left(\frac{v}{u}\right) + au - \frac{u^2+v^2}{2}\right].$$

$$(3)$$

After travelling through the two phase masks, the spatiotemporal vortex tube will be mapped into a photonic toroidal vortex.

The toroidal vortex as a solution to equation (1) in the remapped coordinates can be approximately expressed as

$$\Psi = \left(\frac{\sqrt{(r_\perp - r_0)^2 + \tau^2}}{\sqrt{z_0}}\right)^l \exp\left(-\frac{(r_\perp - r_0)^2 + \tau^2}{2z_0}\right)$$
$$\exp\left(-il\tan^{-1}\left(\frac{\tau}{r_\perp - r_0}\right)\right),$$

$$(4)$$

where $r_\perp = \sqrt{u^2 + v^2}$, r_0 is the radius of the circular vortex line, l is an integer, and z_0 is a constant. Figure 2 shows the iso-intensity
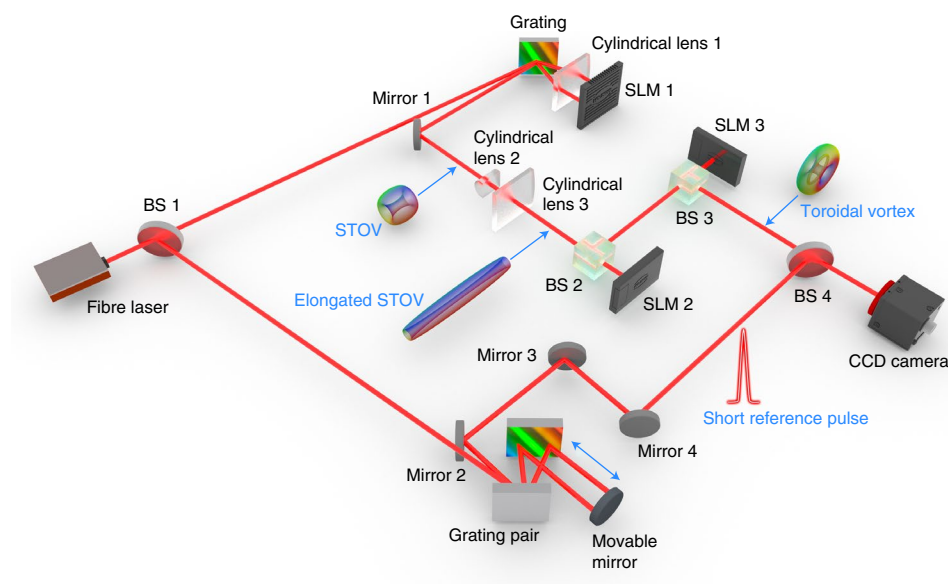
Fig. 3 | Schematic of the experimental apparatus. A chirped pulse from the laser source splits into a signal pulse and a reference pulse. The signal pulse transforms to a spatiotemporal vortex (STOV) pulse after a 2D pulse shaper. The spatiotemporal vortex is stretched along the vortex line and is then converted into a toroidal vortex through an afocal conformal mapping system. The toroidal vortex is characterized by interference with the dechirped reference pulse.
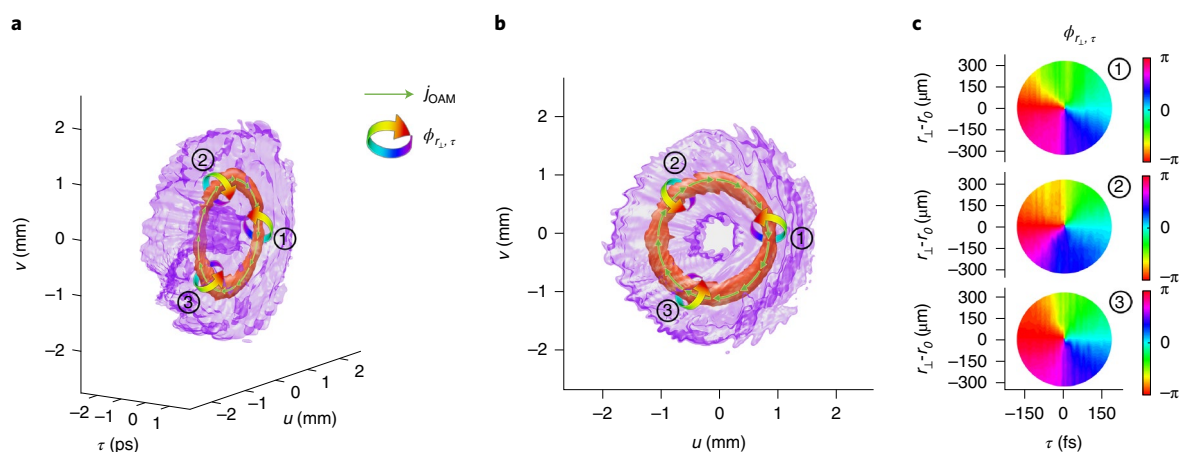

Fig. 4 | Intensity and phase information of an experimentally generated photonic toroidal vortex. a,b, Three-dimensional iso-intensity profile of the photonic toroidal vortex in different views. The maximum intensity is set to 1 and the isovalue is 0.02, meaning that the isosurface profile includes all points with an intensity larger than 0.02. The spatiotemporal spiral phase ($\Phi_{r_\perp}, t$) is marked with curved colourful arrows and the local OAM density (j_{OAM}) is marked with light green arrows. **c,** Circulating spiral phase in the radial–temporal plane. The topological charge of the spiral phase is 1.

surface of a photonic toroidal vortex in different perspective views. The photonic toroidal vortex possesses a 3D phase structure that rotates around a closed loop, forming a ring-shaped vortex line while advancing in the direction perpendicular to the ring orifice at the speed of light. In Fig. 2, the rotating spatiotemporal spiral phase is represented by colours and the direction of local orbital angular momentum (OAM) density is marked with arrows.

The experimental apparatus begins with a dispersion-managed mode-locked fibre laser that emits a chirped pulse (Fig. 3). The light from the source splits into a reference pulse and a signal pulse. The reference pulse is dechirped to a transform-limited pulse through a grating pair. A reflective mirror is mounted on a precision stage after the grating pair so that the path length difference between the reference pulse and the signal pulse can be controlled accurately.

The signal pulse propagates through a 2D pulse shaper that consists of a grating, a cylindrical lens and a reflective programmable spatial light modulator (SLM 1). SLM 1 is situated in the spatial frequency–temporal frequency plane and applies a controlled spiral phase to the signal pulse. After a spatiotemporal Fourier transform, the signal pulse is converted to a wave packet carrying a spatiotemporal vortex[24–27]. The spatiotemporal vortex pulse then travels through an afocal cylindrical beam expander and stretches in the direction of the vortex line. SLM 2 and SLM 3 form an afocal mapping system. They are programmed with the phase profiles as given by equation (2) and equation (3), respectively. Parameters a and b are chosen so that the light occupies a great portion of the liquid-crystal area. The stretched spatiotemporal vortex pulse transforms into a toroidal vortex pulse through the conformal mapping system.

To characterize the 3D field information of the toroidal vortex pulse, the transform-limited reference pulse is combined with the toroidal vortex pulse by a beamsplitter (BS 4) and the interference patterns are recorded by a charged-coupled device (CCD) camera. The reference pulse is considerably shorter (~90 fs) than the toroidal vortex pulse (~3 ps), so, by the use of a precision stage and a movable mirror, the reference pulse interferes with each temporal slice of the toroidal vortex pulse. By utilizing the characterization method[28,29], the amplitude and phase information can be retrieved from the interference patterns. Consequently, the 3D iso-intensity profile of the toroidal vortex pulse can be reconstructed as shown in Fig. 4. Semitransparency is applied so that the ring orifice and the hidden ring-shaped vortex core are clearly shown. The outer layer of the isosurface is coloured in purple and the vortex core surface is coloured in red to make the vortex core stand out. Because the phase gradient is dominant in the radial–temporal plane, the local OAM density direction is at a tangent to the vortex line, as indicated by green arrows. To present the spiral phase rotating about the vortex core, three slices are taken in the radial direction of the ring, as marked numerically (1–3). The phase profiles of the three slices in local coordinates are reconstructed and shown in Fig. 4c. All three images show a spiral phase of topological charge 1. The intensity and phase information demonstrate that the generated pulse is indeed a toroidal vortex. The experiment is carried out in air of very weak positive GVD. The topological charge of the photonic toroidal vortex in the radial–temporal plane is 1, and propagation of the photonic toroidal vortex in air over a short distance will introduce only small distortions. More details on the method and data are provided in Supplementary Figs. 3–7.

In conclusion, we have experimentally demonstrated the generation of a photonic toroidal vortex as a new solution to Maxwell's equations through optical conformal mapping. The preparation of photonic vortex rings is of great importance for studying toroidal electrodynamics, light–matter interactions and photonic symmetry and topology. The concept and conformal mapping method can be readily extended to other spectra, such as electron beams, X-rays and even mechanical waves such as acoustics, hydrodynamics and aerodynamics, opening up new opportunities for studying vortex rings in a wide range of disciplines.

Online content

Any methods, additional references, Nature Research reporting summaries, source data, extended data, supplementary information, acknowledgements, peer review information; details of author contributions and competing interests; and statements of data and code availability are available at https://doi.org/10.1038/s41566-022-01013-y.

References

1. Kilner, P. J. et al. Asymmetric redirection of flow through the heart. *Nature* **404**, 759–761 (2000).
2. Lim, T. & Nickels, T. Instability and reconnection in the head-on collision of two vortex rings. *Nature* **357**, 225–227 (1992).
3. Taddeucci, J. et al. Volcanic vortex rings: axial dynamics, acoustic features, and their link to vent diameter and supersonic jet flow. *Geophys. Res. Lett.* **48**, e2021GL092899 (2021).
4. Hossack, W., Darling, A. & Dahdouh, A. Coordinate transformations with multiple computer-generated optical elements. *J. Mod. Opt.* **34**, 1235–1250 (1987).
5. Berkhout, G. C., Lavery, M. P., Courtial, J., Beijersbergen, M. W. & Padgett, M. J. Efficient sorting of orbital angular momentum states of light. *Phys. Rev. Lett.* **105**, 153601 (2010).
6. Wan, C., Chen, J. & Zhan, Q. Compact and high-resolution optical orbital angular momentum sorter. *APL Photonics* **2**, 031302 (2017).
7. Wen, Y. et al. Spiral transformation for high-resolution and efficient sorting of optical vortex modes. *Phys. Rev. Lett.* **120**, 193904 (2018).
8. Radescu, E. E. & Vaman, G. Exact calculation of the angular momentum loss, recoil force and radiation intensity for an arbitrary source in terms of electric, magnetic and toroid multipoles. *Phys. Rev. E* **65**, 046609 (2002).
9. Ceulemans, A. & Chibotaru, L. F. Molecular anapole moments. *Phys. Rev. Lett.* **80**, 1861–1864 (1998).
10. Lemak, S. et al. Toroidal structure and DNA cleavage by the CRISPR-associated [4Fe-4S]-cluster containing Cas4 nuclease SSO0001 from *Sulfolobus solfataricus*. *J. Am. Chem. Soc.* **135**, 17476–17487 (2013).
11. Thorner, G., Kiat, M., Bogicevic, C. & Kornev, I. Axial hypertoroidal moment in a ferroelectric nanotorus: a way to switch local polarization. *Phys. Rev. B* **89**, 220103 (2014).
12. Miroshnichenko, A. E. et al. Nonradiating anapole modes in dielectric nanoparticles. *Nat. Commun.* **6**, 8069 (2015).
13. Huang, Y. W. et al. Toroidal lasing spaser. *Sci. Rep.* **3**, 1237 (2013).
14. Fedotov, V. A., Rogacheva, A. V., Savinov, V., Tsai, D. P. & Zheludev, N. I. Resonant transparency and non-trivial non-radiating excitations in toroidal metamaterials. *Sci. Rep.* **3**, 2967 (2013).
15. Watson, D. W., Jenkins, S. D., Ruostekoski, J., Fedotov, V. A. & Zheludev, N. I. Toroidal dipole excitations in metamolecules formed by interacting plasmonic nanorods. *Phys. Rev. B* **93**, 125420 (2016).
16. Bao, Y., Zhu, X. & Fang, Z. Plasmonic toroidal dipolar response under radially polarized excitation. *Sci. Rep.* **5**, 11793 (2015).
17. Papasimakis, N., Fedotov, V., Savinov, V., Raybould, T. & Zheludev, N. Electromagnetic toroidal excitations in matter and free space. *Nat. Mater.* **15**, 263–271 (2016).
18. Thomson, W. On vortex atoms. *Phil. Mag.* **34**, 15–24 (1867).
19. Yao, J. & Lundgren, T. Experimental investigation of microbursts. *Exp. Fluids* **21**, 17–25 (1996).
20. Donnelly, C. et al. Experimental observation of vortex rings in a bulk magnet. *Nat. Phys.* **17**, 316–321 (2021).
21. Leonhardt, U. Optical conformal mapping. *Science* **312**, 1777–1780 (2006).
22. Xu, L. & Chen, H. Conformal transformation optics. *Nat. Photon.* **9**, 15–23 (2015).
23. Borovkova, O. V., Kartashov, Y. V., Lobanov, V. E., Vysloukh, V. A. & Torner, L. General quasi-nonspreading linear three-dimensional wave packets. *Opt. Lett.* **36**, 2176–2178 (2011).
24. Sukhorukov, A. & Yangirova, V. Spatio-temporal vortices: properties, generation and recording. *Proc. SPIE* **5949**, 594906 (2005).
25. Hancock, S., Zahedpour, S., Goffin, A. & Milchberg, H. Free-space propagation of spatiotemporal optical vortices. *Optica* **6**, 1547–1553 (2019).
26. Chong, A., Wan, C., Chen, J. & Zhan, Q. Generation of spatiotemporal optical vortices with controllable transverse orbital angular momentum. *Nat. Photon.* **14**, 350–354 (2020).
27. Bliokh, K. Y. Spatiotemporal vortex pulses: angular momenta and spin–orbit interaction. *Phys. Rev. Lett.* **126**, 243601 (2021).
28. Li, H., Bazarov, I. V., Dunham, B. M. & Wise, F. W. Three-dimensional laser pulse intensity diagnostic for photoinjectors. *Phys. Rev. ST Accel. Beams* **14**, 112802 (2011).
29. Chen, J. et al. Automated close loop system for three-dimensional characterization of spatiotemporal optical vortex. *Front. Phys.* **9**, 31 (2021).

Methods

The laser source is a dispersion-managed mode-locked fibre laser with a central wavelength of 1,030 nm. As shown in Fig. 3, a chirped pulse emitted from the laser source is split by a beamsplitter (BS 1). One split pulse passes through a 2D reflective pulse shaper that consists of a grating, a cylindrical lens and a SLM positioned in a 4f configuration. The SLM is a GAEA-2-NIR-069 made by Holoeye. A spiral phase pattern is displayed on the SLM. The phase singularity point of the spiral phase pattern is aligned with the centre of the incident pulse. The 2D pulse shaper turns a Gaussian pulse into a STOV that has a spiral phase in the x–t plane. The STOV is elongated along the vortex line direction (y direction) and becomes a spatiotemporal tube. SLM 2 and SLM 3 are loaded with the phase patterns described by equations (2) and (3), respectively. The two SLMs perform the conformal mapping and transform the spatiotemporal tube into a toroidal vortex. The other pulse split from the laser source is dechirped by a grating pair mounted on an electrically controlled precision stage (Zolix MAR20-65) with a scan step of 5 μm. The transform-limited pulse is utilized as the probe pulse to interfere with each temporal slice of the toroidal vortex. The intensity and phase information of each temporal slice is retrieved from the interference fringe pattern. The 3D isosurface plot is reconstructed through stitching of the 2D temporal slice information.

Data availability

Extra data for this study are available in the Supplementary Information.

Author contributions

C.W., A.C. and Q.Z. proposed the original idea and performed the theoretical analysis. C.W. performed all experiments and data analysis. Q.C. and J.C. contributed to developing the measurement method. Q.Z. guided the theoretical analysis and supervised the project. All authors contributed to writing the manuscript.

Competing interests

The authors declare no competing interests.

Additional information

Supplementary information The online version contains supplementary material available at https://doi.org/10.1038/s41566-022-01013-y.

Correspondence and requests for materials should be addressed to Andy Chong or Qiwen Zhan.

Peer review information *Nature Photonics* thanks Daniele Faccio and Lorenzo Marrucci for their contribution to the peer review of this work.

Reprints and permissions information is available at www.nature.com/reprints.